

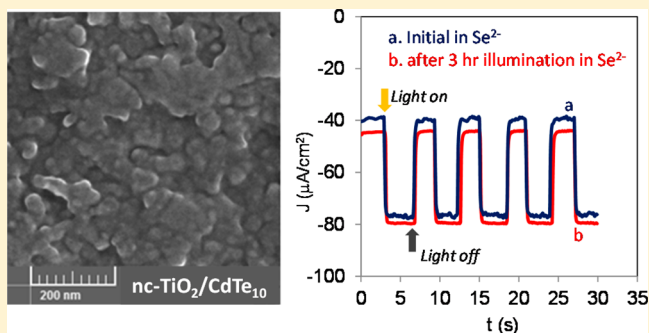
Quantum-Confined CdTe Films Deposited by SILAR and Their Photoelectrochemical Stability in the Presence of Se^{2-} as a Hole Scavenger

Fatima Haydous and Lara Halaoui*

Department of Chemistry, American University of Beirut, Beirut 110236, Lebanon

S Supporting Information

ABSTRACT: Quantum-confined CdTe films were deposited by successive ionic layer adsorption and reaction (SILAR) on nc-TiO₂ and on a conducting oxide electrode (FTO) from aqueous solutions of Cd²⁺ and Te²⁻ prepared in situ under inert atmosphere. The films were characterized with UV–visible absorption, SEM, EDX, and XRD. CdTe_n films exhibited a zinc-blende structure and a red-shift in absorbance with increasing SILAR cycles (*n*) consistent with quantum size effects and featured either a mesoporous morphology on FTO or followed the contours of the titania nanoparticles on nc-TiO₂ films. The films' photoelectrochemical behavior was studied in the presence of Se²⁻ compared to S²⁻ as hole scavengers. The incident-photon-to-current conversion efficiency reached ca. 16% at 460 nm and 9% at 500 nm at CdTe₁₀/nc-TiO₂ in alkaline Se²⁻ electrolyte compared to 1% at 460 nm or 0.5% at 500 nm in S²⁻. CdTe₁₀ films examined after acquiring a photoaction spectrum in Se²⁻ still exhibited zinc-blende structure, EDX analysis showed Cd and Te peaks and no detectable Se, and the absorbance slightly increased with films remaining red-black. On the other hand, the absorbance edge and photocurrent onset shifted significantly to the blue and the films became yellow during the same measurement in S²⁻, indicating dissolution and formation of CdS, consistent with reports for CdTe single crystals and Q-CdTe. After hours of illumination at 500 nm at -0.55 V in Se²⁻, Se became incorporated in the films; however, the photocurrent decreased by only 5–8% after 2–3 h illumination, indicating significant photoelectrochemical stability. The results are attributed to effective quenching of the anodic dissolution of CdTe by Se²⁻ scavenging the hole, and a slow growth of a protective overlayer possibly of CdTe_{1-x}Se_x that does not block photocurrent generation, in contrast to the behavior of CdTe in sulfide electrolyte.



INTRODUCTION

Quantum dots (QD) have attracted significant research interest because they hold the promise of increasing the efficiency and reducing the cost of power from photovoltaics in third-generation solar cells.¹ QDs are nanoparticles with dimensions comparable to the semiconductor exciton diameter. They offer the advantages of tunable band gap and band edges,² high extinction coefficients,^{2,3} and large intrinsic dipole moment.^{4,5} Central to their promise is a theoretical prediction that the Shockley–Quieser thermodynamic limit of 31% for conversion of light to chemical or electrical energy at a single junction can be exceeded in QD solar cells,¹ by improving photovoltage via hot carrier transfer or photocurrent via multiple exciton generation (MEG) or carrier multiplication.^{6–11} Despite earlier controversy surrounding MEG in QD films, experimental evidence of its occurrence continued to be reported.^{7–11}

Quantum dots have been incorporated in solar cells in different configurations including blending with conducting polymers,^{12,13} in QD films with a liquid junction,¹⁴ in QD film/metal Schottky junction,^{15,16} or in QD-sensitized solar cells (QDSSC).^{17,18} In QDSSCs, QDs sensitize a wide band gap metal oxide such as TiO₂ or ZnO. Several QDs have been

employed including CdS and CdSe, yet the overall power conversion efficiency remains below 5%.^{17,19,20} The factors that affect these cells' efficiency include the absorption range, the rates of electron transfer to the conduction band of the metal oxide and hole transfer to the redox species, the QD photostability in the liquid medium, and e-h recombination in the films, at interfaces, or via the redox species.^{21,22}

Cadmium telluride, a direct II–VI semiconductor with an energy gap of 1.45 eV well matched to the solar spectrum is a highly stable material when used in photovoltaic solid-state devices. CdTe solid-state PV technology is second only to crystalline silicon on the world market. Because of a band gap smaller than that of CdSe (1.74 eV) and CdS (2.4 eV), CdTe is of interest in QDSSC, but stabilizing it against anodic photooxidation has been a challenge. The hole in II–VI semiconductors such as CdS, CdSe, and CdTe can attack the lattice itself in the absence of a sacrificial hole scavenger in solution. While both CdS and CdSe can be stabilized using

Received: April 23, 2014

Revised: June 27, 2014

Published: July 30, 2014

sulfide/polysulfide, CdTe cannot be. Kamat et al. reported that Q-CdTe/nc-TiO₂ films were unstable in sulfide, with a %IPCE of ~0.3% at 500 nm, attributed to the formation of a CdS layer that blocks photocurrent generation.²¹ Early studies by Wrighton and co-workers also showed that S²⁻ is not a suitable hole scavenger for CdTe single crystals, but that both Se²⁻ and Te²⁻ quench the dissolution.²³ Kamat and co-workers reported attempting different redox couples with Q-CdTe/TiO₂ such as I⁻/I₃⁻, ferrocene/ferrocene⁺, K₄Fe(CN)₆/K₃Fe(CN)₆, and Te²⁻/Te₂²⁻ but that none gave the required photostability.²¹ Finding a suitable redox couple that can stabilize Q-CdTe is essential for its use in photoelectrochemical cells.

Approaches to sensitize metal oxides with QDs have included linker-assisted adsorption of colloidal QDs,^{17,24,25} electrochemical deposition,²⁶ electrophoresis,^{24,27} chemical bath deposition (CBD)^{28,29} where the precursors are mixed in one medium, and successive ionic layer adsorption and reaction (SILAR) where the electrode is dipped successively into each of the precursor solutions.^{30,31} SILAR does not introduce a linker distance, can offer better control of particle size and amount relative to CBD,³² and is suitable for multilayer assembly.³³ One challenge in depositing metal selenide and telluride by SILAR is to stabilize the Se²⁻ or Te²⁻ ions against oxidation. Lee et al. deposited Q-CdSe on TiO₂ using SILAR by preparing Se²⁻ in ethanol from SeO₂ and reducing it under inert atmosphere and similarly deposited a layer of CdTe on CdSe starting from TeO₂ in ethanol.³¹ We utilized a modified procedure starting from Se powder in ethanol to sensitize TiO₂ inverse opals and nc-TiO₂ with CdSe by SILAR.³⁴ To our knowledge to date, there has been no reported application of SILAR to sensitize mesoporous oxides with CdTe.

In this paper, we report the deposition of quantum-confined CdTe films by SILAR and the photoelectrochemical film stability in alkaline Se²⁻ electrolyte. CdTe films were deposited on nc-TiO₂ and on conducting oxide electrode (FTO) from aqueous solutions of Cd²⁺ and Te²⁻ prepared in situ from Te(s) reduced with sodium borohydride under inert atmosphere. The films were characterized with UV-visible absorption, SEM, EDX, and XRD, and their photoelectrochemical behavior was studied in alkaline Se²⁻ electrolyte prepared in situ from Se and sodium borohydride in comparison with alkaline sodium borohydride and alkaline sulfide electrolyte solutions. While sulfide is not a suitable hole scavenger leading to anodic dissolution of CdTe in agreement with reported studies of Q-CdTe and CdTe single crystals, CdTe films exhibited significant stability and photocurrent generation in the presence of selenide that were not observed in its absence. The results are attributed to efficient quenching of anodic dissolution by Se²⁻ scavenging the hole, and a slow dissolution and substitution resulting in an overlayer possibly of CdTe_{1-x}Se_x that may have protected the surface against further dissolution without blocking photocurrent generation, in contrast to the behavior of CdTe in sulfide.

RESULTS

CdTe films were deposited by dipping nc-TiO₂ or FTO electrodes successively in Cd²⁺(aq) and Te²⁻(aq) solutions under inert atmosphere. The Te²⁻ precursor solution was prepared in situ by reacting Te(s) with sodium borohydride in alkaline aqueous solution under nitrogen and was stabilized by maintaining a nitrogen blanket during deposition. The films will be denoted CdTe_n, with *n* referring to the SILAR cycle number. Figure 1 shows UV-vis absorption spectra of CdTe deposited

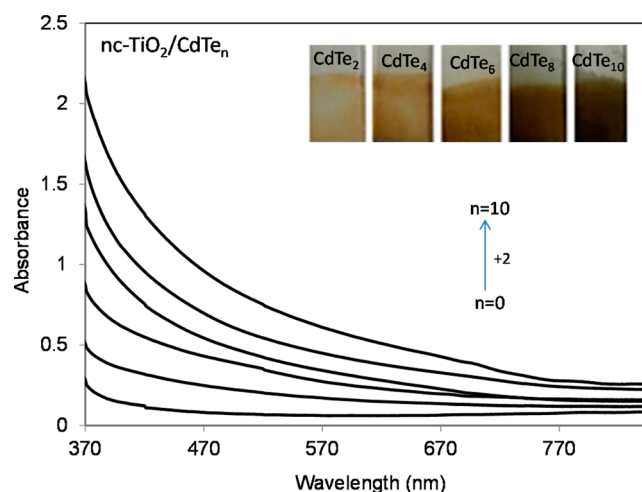
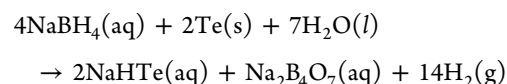


Figure 1. UV-visible absorbance spectra of CdTe_n deposited on nc-TiO₂ with *n* = 2, 4, 6, 8, 10 SILAR cycles and of nc-TiO₂ before sensitization. The inset shows photos of CdTe_n films with increasing SILAR cycles.

by 2 to 10 cycles on nc-TiO₂. The films' absorption edge was blue-shifted from CdTe bulk absorption (edge at 855 nm), indicating quantization effects. The spectra show increased absorbance with increasing *n* up to this layer number and a red shift in the absorption edge as expected from quantum size effects. CdTe_n films ranged in color from yellow-orange for CdTe₂ to very deep red-black for CdTe₁₀ (inset of Figure 1). As expected, the CdTe films were stable in air. Figure S1 in Supporting Information presents UV-visible absorbance spectra of CdTe₁₀ deposited on FTO directly after deposition and after sitting 3 days in air. Different from the deposition of CdSe by SILAR from ethanolic precursor solutions, dipping in precursor solutions in ethanol did not lead to CdTe deposition. Klayman et al. reported that Te reacts slowly with sodium borohydride in water, possibly forming sodium hydrogen telluride, but is not reactive in ethanol, while Se is reactive.³⁵ The reaction leading to the formation of Te²⁻ may be written as



The absorbance of independently deposited CdTe₁₀ films on nc-TiO₂ (*N* = 7) from different solutions was examined to assess the reproducibility of the SILAR process. The absorbance at 600 nm of nc-TiO₂/CdTe₁₀ (*N* = 7) ranged between 0.42 and 0.69 with an average absorbance of 0.53 ± 0.10, and the absorbance at 400 nm ranged between 1.4 and 2.7 with an average of 1.86 ± 0.46. The CdTe₁₀ films exhibited the same absorption edge, and some featured a shoulder in their absorption spectrum at ~700 nm. Despite the variation, CdTe_n films deposited in an experiment from the same solution with increasing SILAR cycle number (*n*) exhibited an increase in the optical density with increasing *n* and a red-shift in the absorbance edge.

SEM images and EDX spectra of CdTe₁₀ on FTO and nc-TiO₂ are presented in Figure 2. CdTe₁₀ films on FTO exhibited a nanoporous structure, and the underlying FTO is seen to consist of nanoscale island structures. CdTe₁₀ films on nc-TiO₂ appeared as a compact film that seemingly followed the surfaces of the 13 nm TiO₂ particles. The outlines of underlying

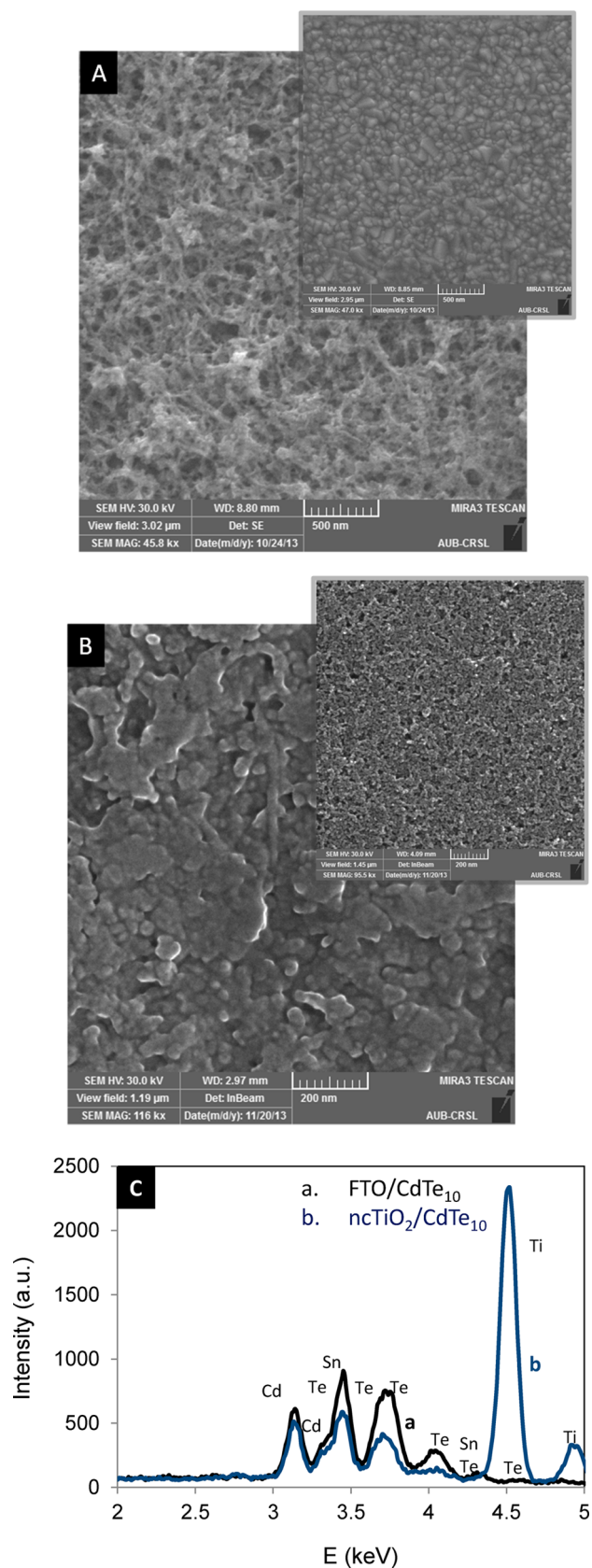


Figure 2. (A) SEM image of CdTe₁₀ deposited on FTO, and SEM image of FTO in the inset. (B) SEM image of CdTe₁₀ deposited on nc-TiO₂, and an SEM image of the nc-TiO₂ film before sensitization. (C) EDX spectra of CdTe₁₀/FTO (black trace, a) and CdTe₁₀/nc-TiO₂ (blue trace, b).

particles can be seen in SEM images underneath the surface film. The substrate morphology must have determined the architecture by affecting the initial seed layer and nucleation. CdTe must have deposited on the surface of TiO₂ particles when the precursor solutions infiltrated the interstitial space between nanoparticles. EDX elemental analysis of CdTe₁₀ on FTO and nc-TiO₂ showed Cd and Te peaks, confirming CdTe deposition. XRD spectra of CdTe₁₀ on FTO and on nc-TiO₂ are presented in Figure 3, showing peaks corresponding to (111), (210), (311), (331), and (422) diffractions of CdTe zinc-blende structure.

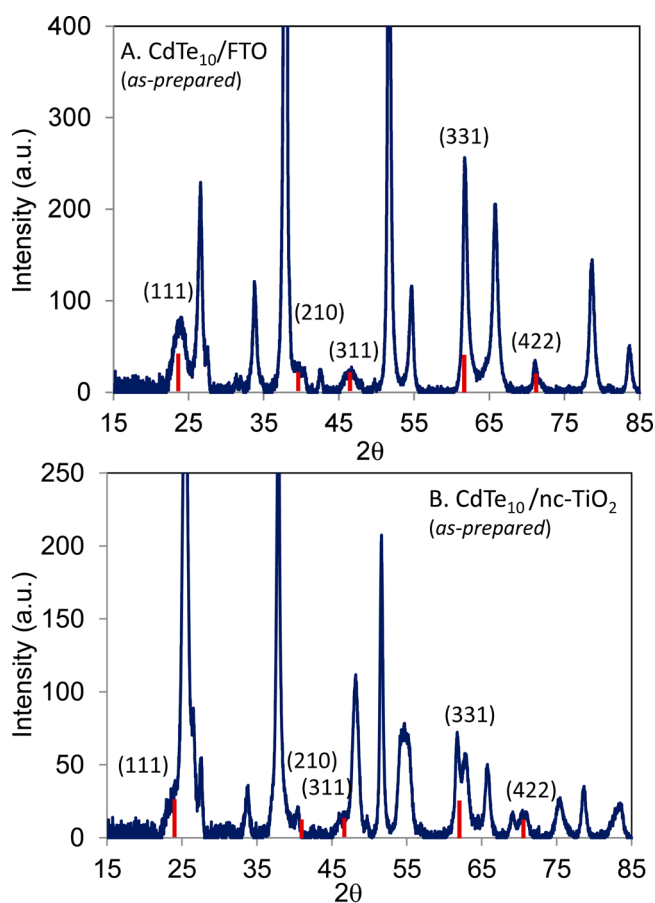


Figure 3. XRD spectra of CdTe₁₀/FTO (A) and CdTe₁₀/nc-TiO₂ (B) as prepared. The red lines indicate the positions of the (111), (210), (311), (331), and (422) XRD diffraction peaks of zinc-blende CdTe.

The same mechanism believed to take place for deposition of CdSe and CdS by SILAR can be thought to occur here. During the first cycle, Cd²⁺ ions adsorb on nc-TiO₂ particles or on FTO. When dipped in the telluride solution, Te²⁻ ions react with the adsorbed Cd²⁺ layer to form a CdTe seed layer directly contacting the substrate. Following this wetting step, Cd²⁺ and Te²⁻ ions accumulate on the CdTe seed layer and nucleation starts followed by growth of small dots.^{32,36} The increase in the number of cycles was reported to lead to increased coverage of larger size quantum dots.³⁷ Thicker films and increasing the nanoparticle dimensions are expected to lead to the observed red shift in absorbance with more SILAR cycles.

The photoelectrochemical behavior of CdTe-sensitized nc-TiO₂ and FTO was studied in alkaline Se²⁻ electrolyte prepared in situ under nitrogen from Se(s) and sodium borohydride, and the behavior was compared to that in alkaline sulfide. Figure S2

in Supporting Information shows chronoamperometric curves under chopped illumination at 440 and 540 nm at CdTe₁₀/nc-TiO₂ biased at -0.55 V vs Ag/AgCl in both electrolytes. The traces show the absence of detectable photocurrent at 540 nm and a small photocurrent at 440 nm in sulfide and significantly greater photocurrents in Se²⁻. This revealed Se²⁻ to be more efficient in scavenging the CdTe photogenerated holes.

Figure 4 shows photoaction spectra (%IPCE vs wavelength) collected at CdTe₅, CdTe₁₀, and CdTe₁₅ sensitized nc-TiO₂ in

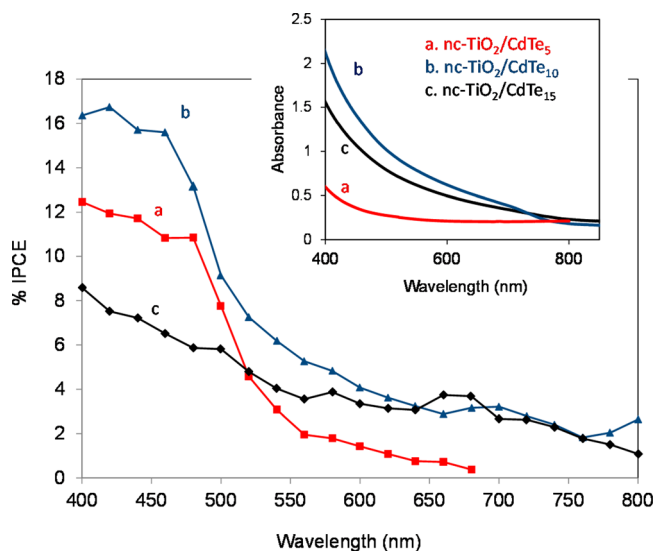


Figure 4. Photoaction spectra (%IPCE vs wavelength) at CdTe₅ (a), CdTe₁₀ (b), and CdTe₁₅ (c) sensitized nc-TiO₂ films in deaerated alkaline Se²⁻ electrolyte. The inset shows the absorbance spectra of the films.

Se²⁻, and the inset shows the corresponding absorbance spectra of the same CdTe₅, CdTe₁₀, and CdTe₁₅ films. The %IPCE value was about 4.8% at CdTe₅/nc-TiO₂ and ca. 7.3% at CdTe₁₀/nc-TiO₂ at 520 nm, and 10.8% and 15.6% at 460 nm at the two films, respectively. The photocurrent onset occurred between 560 and 620 nm at CdTe₅ and was red-shifted to 800 nm at CdTe₁₀, consistent with the absorption edges. A shoulder appeared at ~ 700 nm in this CdTe₁₀ film absorption spectrum, possibly corresponding to an excitonic transition and possibly translated as a small shoulder-peak in the photoaction spectrum. The absence of a shift in the photocurrent onset from the absorption edge indicated the films' integrity during the photoelectrochemical measurement and that the photocurrents resulted from an initial absorption event in CdTe without significant dissolution that would lead to absorbance edge shift.

The %IPCE decreased to $\sim 5\%$ at 520 nm and $\sim 7\%$ at 460 nm at 15 layers (CdTe₁₅). The photocurrent onset, however, remained at about 800 nm, similar to CdTe₁₀. The absorption spectra show lower absorbance for CdTe₁₅ than for CdTe₁₀ and a slightly red-shifted absorption edge (inset of Figure 4). The lower absorbance for CdTe₁₅ at short wavelengths could be attributed to larger particles in thicker films after filling the pores, but the %IPCE is lower than can be accounted for by the lower absorbance. This must indicate greater charge recombination in thicker CdTe₁₅ films that could result from lower efficiency of hole scavenging if the electrolyte cannot reach the internal surface and lower efficiency of electron injection to TiO₂ when CdTe layers are beyond an optimal thickness. Lee

et al. also reported that the conversion efficiency was saturated at six SILAR layers of CdSe.³¹

Figure S3 in Supporting Information shows UV–visible absorbance spectra of CdTe₁₀/nc-TiO₂ as deposited and after acquiring a photoaction spectrum in Se²⁻, which consisted of 5 min total illumination at -0.55 V between 400 and 800 nm. A small increase in absorbance is shown in the latter case without a shift in absorbance edge, while the film remained red-black (inset). Figure 5 presents XRD patterns of CdTe₁₀/FTO and

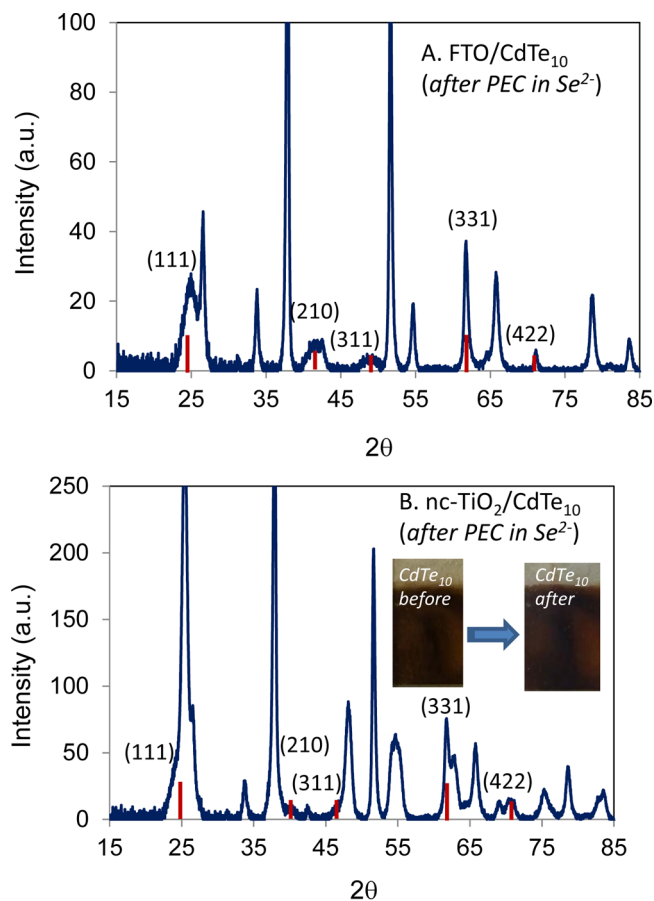


Figure 5. XRD spectra of CdTe₁₀/FTO (A) and CdTe₁₀/nc-TiO₂ (B) acquired after acquiring a photoaction spectrum in deaerated alkaline Se²⁻ electrolyte. (These are the same films with XRD spectra in the as-prepared state in Figure 3). The red lines indicate the positions of the (111), (210), (311), (331), and (422) XRD diffraction peaks of zinc-blende CdTe. The inset of B shows photos of red-black CdTe₁₀/nc-TiO₂ films before and after the photoelectrochemical experiment in Se²⁻.

CdTe₁₀/nc-TiO₂ after acquiring a photoaction spectrum, showing the same diffraction peaks characteristic of cubic CdTe (same films as presented in Figure 3 in the as-prepared state), with no new peaks appearing. EDX elemental analysis (Figure S4, Supporting Information) showed clear Cd and Te peaks, and no Se peaks were detected above the background after the measurement in Se²⁻. Se peaks, however, appeared with longer illumination. Figure 6 shows the EDX spectrum of a CdTe₁₀/nc-TiO₂ film after ~ 3 h (2 h 52 min) illumination at 500 nm in Se²⁻ at -0.55 V. In addition to Cd and Te peaks, an intense Se peak appeared at 1.3 keV and smaller peaks at 11.2 and 12.3 keV. The film became a lighter orange-red color. Photocurrent generation in selenide electrolyte, however, did

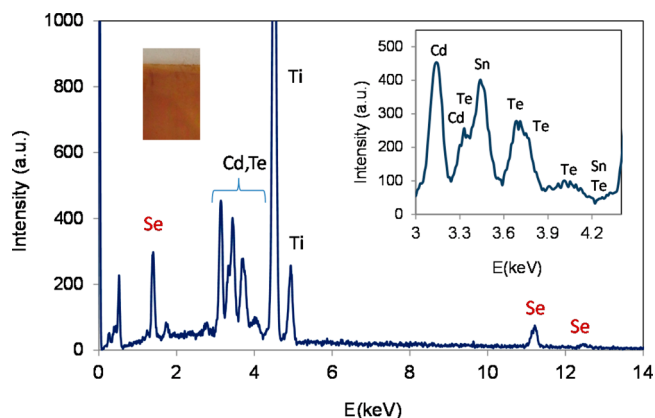


Figure 6. EDX spectrum of CdTe₁₀/nc-TiO₂ film after 2 h S₂²⁻ illumination at 500 nm at -0.55 V vs Ag/AgCl in deaerated alkaline S₂²⁻ electrolyte. The insets show the Cd and Te peaks in the EDX spectrum, and a photograph of the film after the experiment.

not appreciably decline with time. Figure 7 shows an initial *i*-*t* curve under chopped illumination at CdTe₁₀/nc-TiO₂ in S₂²⁻

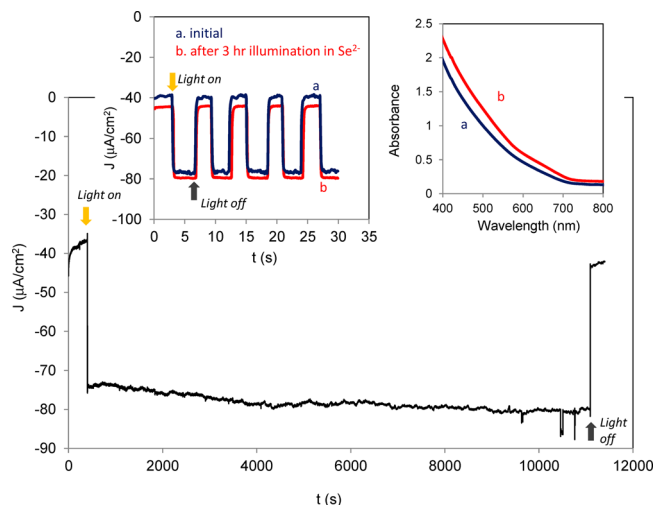


Figure 7. Chronoamperometry plot at a CdTe₁₀/nc-TiO₂ biased at -0.55 V vs Ag/AgCl in deaerated alkaline S₂²⁻ electrolyte during ca. 3-h continuous illumination at 500 nm. The left inset show *i*-*t* curves acquired initially (a, blue) and after the continuous illumination (b, red), at 500 nm at -0.55 V vs Ag/AgCl in deaerated alkaline S₂²⁻ electrolyte under chopped illumination. The right inset shows absorbance spectra of the film before (a, blue) and after the photoelectrochemical experiment (b, red).

at -0.55 V, followed by illumination for ca. 3 h at a bias of -0.55 V, and an *i*-*t* curve under chopped illumination at the end of the experiment. The photocurrent decreased by only 5% from its initial value. The absorbance spectra of the film before and after illumination (inset) reveal a similar absorbance onset and a small absorbance increase. Two other independently prepared CdTe₁₀/nc-TiO₂ films exhibited a 7.5% or 7.8% decrease in photocurrent at 500 nm after 2 or 3 h illumination, respectively.

To investigate whether introducing Se can increase film absorbance, two CdTe₁₀ films were deposited from the same medium and one of them was capped with a top layer of CdSe (termed CdTe₁₀CdSe₁); Figure S5 in Supporting Information shows their photoaction and absorbance spectra. The films

exhibited similar photocurrent conversion efficiency and photocurrent onset and the same absorption onset but with greater absorption by CdTe₁₀CdSe₁. This is similar to the increase in absorbance of CdTe₁₀ after illumination in S₂²⁻.

The photoaction spectrum measured at CdTe₁₀/nc-TiO₂ in alkaline sodium borohydride in the absence of Se showed about half the %IPCE values measured in the presence of S₂²⁻ (Figure S6 in Supporting Information for two CdTe₁₀ films deposited in the same medium). Illumination under the same conditions in alkaline sodium borohydride in the absence of S₂²⁻ resulted in a 74% drop in photocurrent after 2 h illumination at -0.55 V at 500 nm with a fast initial decrease (Figure S7, Supporting Information). The films changed color to very light yellow-orange (Figure S7), and the absorbance significantly decreased (Figure S8, Supporting Information).

The photoelectrochemical behavior in S₂²⁻ indicated a stability that is in contrast to that in alkaline S₂²⁻. Figure 8

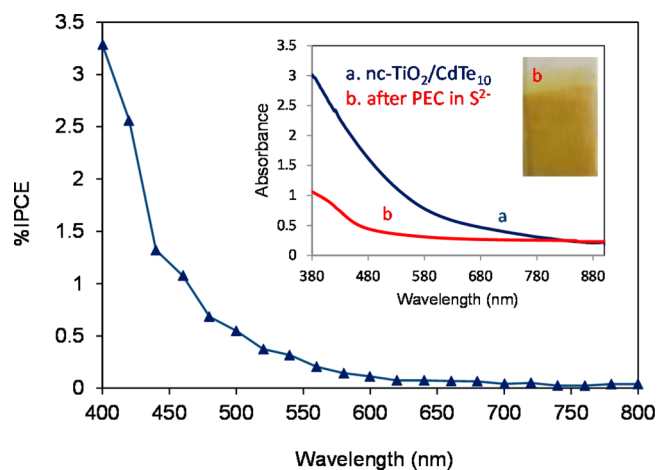


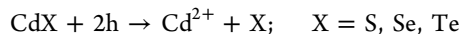
Figure 8. Photoaction spectrum of CdTe₁₀/nc-TiO₂ in deaerated alkaline sulfide electrolyte. The inset shows absorbance spectra of the film before (a, blue) and after (b, red) acquiring a photoaction spectrum in S₂²⁻ electrolyte, along with a photograph of the yellow colored film after the experiment.

presents a photoaction spectrum at CdTe₁₀/nc-TiO₂ in sulfide, showing a %IPCE of 0.5% at 500 nm compared to 9% in S₂²⁻, or 1.1% at 460 nm compared to ca. 16% in S₂²⁻. The absorbance decreased significantly after acquiring a photoaction spectrum in this electrolyte, with the absorption edge shifting to the blue, and the film color changed from deep red-black to yellow (inset of Figure 8), indicating significant anodic dissolution. These results are consistent with the study of Kamat et al. of 3.2 nm Q-CdTe dots linker-adsorbed on nc-TiO₂ where the %IPCE in sulfide was about 0.3% at 500 nm.²¹ The authors attributed the low %IPCE to CdS growth on Q-CdTe, blocking photocurrent generation.²¹

The presence of nc-TiO₂ facilitates charge separation and transport. Figure S9 in Supporting Information presents photoaction spectra at CdTe₁₀/FTO and CdTe₁₀CdSe₁/FTO in S₂²⁻, showing a %IPCE not exceeding 1% at 440 nm, despite appreciable absorbance (inset). Although the nanoporous structure of CdTe₁₀/FTO would allow for sufficient infiltration of the electrolyte, the long transport distance to FTO results in inefficient charge separation, coupled with a greater interface for back electron reaction. The nanoporous CdTe films on FTO may, however, be of interest in other systems because of an open structure that may be filled.

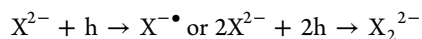
DISCUSSION

Cadmium chalcogenide electrodes are susceptible to anodic dissolution under illumination according to the following reaction:



This instability is a major challenge facing the investigation of the photoelectrochemical behavior of CdTe QDs and their incorporation in liquid junction solar cells.

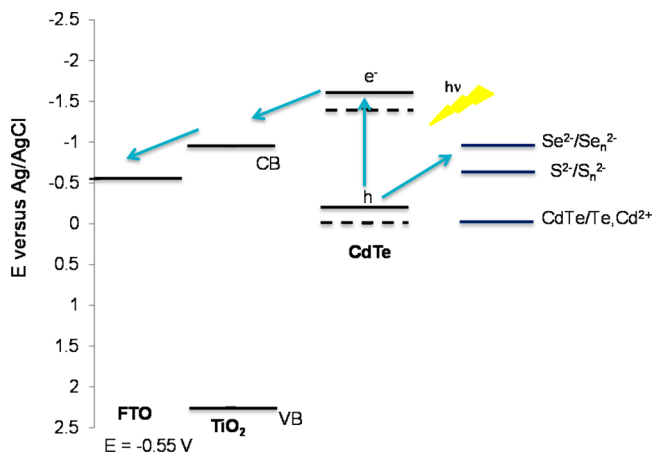
The electrodes may be protected in the presence of a suitable redox species X^{2-} that can scavenge the hole according to



When both reactions are thermodynamically feasible, the photoelectrode stability will depend on the kinetic facility of these two competing reactions. Wrighton and co-workers studied CdX single crystals in the presence of $\text{X}^{2-}/\text{X}_n^{2-}$ redox couples using different combinations of X and observed that CdS and CdSe photoelectrodes are stable in sulfide but that a fast decrease in photocurrent occurs at CdTe in this electrolyte and an insoluble orange-yellow layer forms on the illuminated surface (at -0.9 V vs SCE).²³ On the other hand, CdTe single crystals were stable in the presence of Se^{2-} or Te^{2-} .²³ Kamat et al. observed that Q-CdTe is unstable in sulfide and that the QDs lacked the required stability with other redox couples that included Te^{2-} .²¹ In this study, quantum-confined CdTe films deposited by SILAR were shown to exhibit significant stability in Se^{2-} compared to S^{2-} electrolyte.

Scheme 1 shows the energy diagram of CdTe/TiO₂ on FTO in $\text{Se}^{2-}/\text{Se}_n^{2-}$ solution, with energy levels taken as reported by

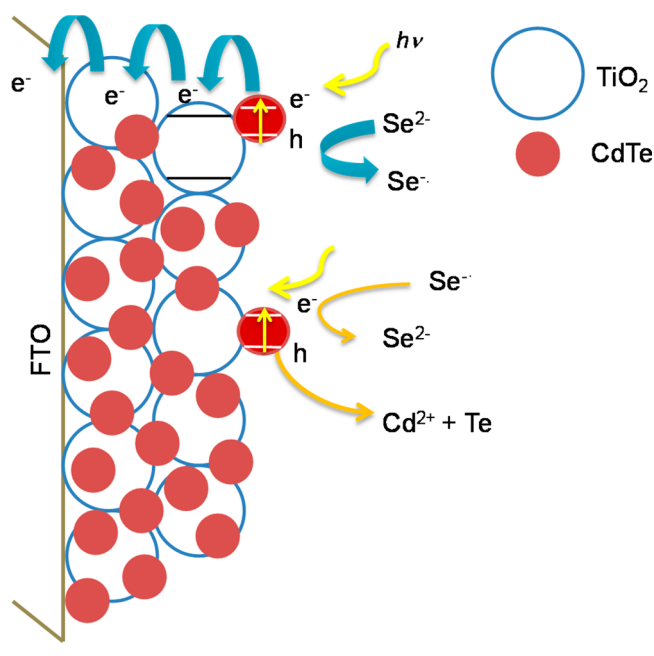
Scheme 1. Energy Level Diagram of CdTe/nc-TiO₂ on FTO in $\text{Se}^{2-}/\text{Se}_n^{2-}$, with Energy Levels Taken As Reported by Ellis et al.^{23a}



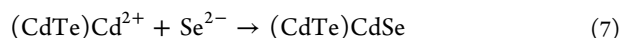
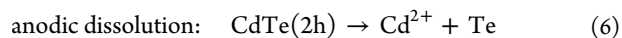
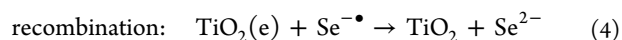
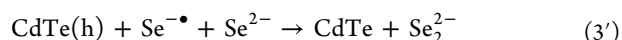
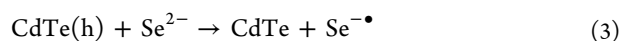
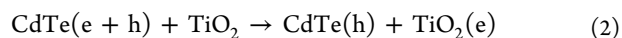
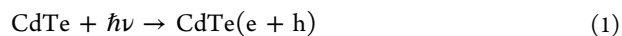
^aThe solid and dashed lines are numbers reported using two different measurements (photocurrent–voltage (solid) and Mott–Schottky plots (dashed)) from ref 23.

Ellis et al.,²³ and Scheme 2 shows the main charge transfer processes. Upon visible light absorption by CdTe, electrons and holes are photogenerated (reaction 1), and fast electron injection occurs from CdTe into the conduction band of TiO₂ (reaction 2). Electron injection from (3.2 nm) Q-CdTe to nc-TiO₂ has been reported to occur with an apparent rate constant of $2.1 \times 10^9 \text{ s}^{-1}$, 1 order of magnitude greater than the rate of $2.4 \times 10^8 \text{ s}^{-1}$ from (3 nm) Q-CdSe to nc-TiO₂.³⁸ It was

Scheme 2. The Main Charge Transfer Processes at CdTe/nc-TiO₂ on FTO in the Presence of Se^{2-}



noted that a significant injection fraction also occurs with a faster component up to 10^{10} s^{-1} .²¹ This separates the charges. The photohole can be scavenged by Se^{2-} (reactions 3, 3'), which can first lead to $\text{Se}^{\bullet-}$ and then Se_2^{2-} upon scavenging of another hole. The fate of the separated photoelectron can be either to recombine with the hole at the interface, to undergo back-electron transfer reaction with the oxidized redox couple (e.g., reaction 4), or transfer to the underlying electrode generating a photoanodic current (reaction 5). To increase the power conversion efficiency, the recombination step via the redox couple should be suppressed and will be more significant in the presence of the oxidized form of the couple.



The photohole can also react with the lattice, leading to photoanodic dissolution (reaction 6). For the anodic dissolution reaction to be thermodynamically feasible, the valence band edge (E_{VB}) must be more positive than the redox potential of reaction 6. The reduction potential of the reaction $\text{Te} + 2e + \text{Cd}^{2+} \rightarrow \text{CdTe}$ is reported at -0.14 V vs SCE, and E_{VB} of CdTe in selenide was measured at -0.25 V or -0.05 V from current–voltage or Mott–Schottky plots, respectively.²³ The numbers indicated that the photoanodic dissolution of CdTe in selenide may be thermodynamically unfavorable (if

$E_{VB} = -0.25$ V) or favorable (if $E_{VB} = -0.05$ V) with a small driving force (90 mV built-in overpotential) relative to the built-in overpotential for hole scavenging by Se^{2-} (E of $\text{Se}^{2-}/\text{Se}_n^{2-}$ is -0.95 V vs SCE). Although quantum confinement increases the energy gap, the increase in the energy of the hole is not expected to be major for CdTe_{10} . The absorption edge at 800 nm corresponds to an energy gap of 1.55 eV compared to a band gap of 1.45 eV for bulk CdTe, and the larger effective mass of the hole ($0.35 m_0$)³⁹ relative to the electron ($0.11 m_0$)³⁹ results in most of the shift to be in the position of the CB.

At short illumination time, Se was not detected with EDX, and XRD patterns revealed the stability of cubic CdTe. This stability is attributed to competitive quenching of the anodic dissolution by Se^{2-} scavenging the hole. After long illumination at a bias of -0.55 V in selenide, EDX elemental analysis showed that Se became incorporated in CdTe, indicating some anodic dissolution and substitution, but the photoanodic current decreased by only 5–8% after hours of illumination at 500 nm. The results can be interpreted by proposing a slow substitution of Te with Se on the CdTe surface as a result of initial surface anodic dissolution (reaction 6) that is slowed down by competition from hole scavenging by Se^{2-} . This may be followed by adsorption of dissolved Cd^{2+} and reaction with Se^{2-} , or Te^{2-} reduced from Te produced by (reaction 6), forming an overlayer possibly of $\text{CdTe}_{1-x}\text{Se}_x$ (reaction 7). Because absorbance by CdSe in the bulk ($E_g = 1.74$ eV) does not extend beyond 713 nm, the photocurrent onset of 800 nm at CdTe_{10} in Se^{2-} and the absence of a shift in the absorbance edge indicate that photocurrent generation is still mainly due to absorption by CdTe. The overlayer may have protected the surface against further dissolution, explaining how the absorbance and photocurrent did not appreciably change after hours of illumination. Kamat and co-workers showed that a shell of $\text{CdSe}_{1-x}\text{S}_x$ grows on Q-CdSe in $\text{S}^{2-}/\text{S}_n^{2-}$, but this overlayer does not block photocurrent generation and prevents further corrosion of CdSe.⁴⁰ A similar mechanism can be thought to take place, with the growth of a protective thin $\text{CdTe}_{1-x}\text{Se}_x$ overlayer that allows charge tunneling. In alkaline sodium borohydride solution in the absence of Se, even though %IPCE values were as high as half their values in Se^{2-} initially, the absorbance decreased significantly and the photocurrent dropped by 74% after 2-h illumination with an initial fast decline, indicating significant dissolution. This is evidence that Se^{2-} is quenching the dissolution and that a thin shell may have protected the illuminated CdTe lattice over time in Se^{2-} .

On the other hand, a drastic blue shift in absorbance and in photocurrent onset occurred in sulfide and a minimal %IPCE was measured, with the film turning yellow, consistent with other studies of CdTe single crystals and quantum dots in S^{2-} electrolyte.^{23,40} In sulfide, E_{VB} of CdTe single crystal was reported at -0.10 V from MS plots, making the dissolution thermodynamically favorable.²³ A layer of CdS was reported by Ellis et al. to grow on CdTe single crystals,²³ and this was similarly reported by Kamat et al. for Q-CdTe,²¹ which was thought to block photocurrent generation. Ellis et al. attributed the difference in behavior of CdTe in Se^{2-} and S^{2-} to the $\text{S}^{2-}/\text{S}_n^{2-}$ less negative E_{redox} (at -0.72 V vs SCE).²³ The redox potential of $\text{Se}^{2-}/\text{Se}_n^{2-}$ is 0.23 V more negative than $\text{S}^{2-}/\text{S}_n^{2-}$, and this difference in built-in overpotential can cause the quenching reaction to be faster in selenide.

CONCLUSIONS

We reported in this study that an Se^{2-} electrolyte solution prepared from Se and NaBH_4 under nitrogen can stabilize thin CdTe films in a photoelectrochemical medium. The experiments showed that Se^{2-} is a suitable hole scavenger to protect CdTe and separate the hole. The observed stability is attributed to effective quenching of the anodic dissolution reaction by Se^{2-} scavenging the hole and the possible growth of a protective overlayer of $\text{CdTe}_{1-x}\text{Se}_x$ that does not block generation of photocurrent. The presence of Se^{2-} was essential to the stability, as significant anodic dissolution was observed in alkaline sodium borohydride solution in the absence of Se and in alkaline sulfide solution. This finding opens the possibility of incorporating Q-CdTe in photoelectrochemical cells with using Se^{2-} in an aqueous liquid junction to increase the red visible light response of QDSSC. Future studies are needed to understand the dynamics of hole transfer from CdTe to Se^{2-} compared to the electron injection rate from Q-CdTe thin films to TiO_2 and the rate of the back electron reaction with the oxidized redox species, with the general aim of devising ways to affect the different charge transfer rates to increase the photostability and suppress redox couple-mediated recombination that lower the conversion efficiency of QDSSC.

EXPERIMENTAL METHODS

Materials. Nanocrystalline TiO_2 slurry (nc- TiO_2 , $\langle d \rangle = 13$ nm, Solaronix, Switzerland), cadmium perchlorate hydrate ($\text{Cd}(\text{ClO}_4)_2 \cdot \text{H}_2\text{O}$, Aldrich), tellurium powder (Te, 99.99%, Alfa Aesar), selenium powder (Se, 99.999%, Alfa Aesar), sodium borohydride (NaBH_4 , 98%, Aldrich), 2-propanol (99.5%, Riedel-de Haën), sodium sulfide nonahydrate ($\text{Na}_2\text{S} \cdot 9\text{H}_2\text{O}$, Alfa Aesar), sodium hydroxide (NaOH, Aldrich), and double distilled water were used.

Nanocrystalline TiO_2 Film Preparation. Nanocrystalline TiO_2 (nc- TiO_2) films ($\sim 5 \mu\text{m}$ thick) were deposited using the squeegee method on fluorine-doped SnO_2 glass substrates (FTO, Solaronix) from a slurry of 13 nm TiO_2 (anatase, $E_g = 3.2$ eV). FTO electrodes were cleaned by sonication in 2-propanol for 30 min followed by sonication in water for 20 min in an ultrasonic bath (Nickel Electro Ltd.). One layer of scotch tape (3M) was used as a spacer to control the thickness. The solvent was evaporated at 80°C , and then the films were sintered at 400°C for 1 h.

Deposition of CdTe Films by SILAR. CdTe films were deposited on FTO substrates or on nc- TiO_2 films via multiple cycles of SILAR, by dipping in aqueous solutions of the precursors Cd^{2+} and Te^{2-} . Te^{2-} precursor solutions were prepared in situ under an inert atmosphere to ensure stability against oxidation. For this purpose, 0.062 g of Te powder was reacted with excess NaBH_4 (0.24 g) in 26 mL of water and purged with N_2 (g) for at least 40 min until the solution became colorless. Some Te(s) remained precipitated in the beaker. A $\text{Cd}^{2+}(\text{aq})$ solution was prepared by dissolving 0.24 g of $\text{Cd}(\text{ClO}_4)_2 \cdot \text{H}_2\text{O}$ in 26 mL of water and was deoxygenated by purging with N_2 gas for at least 40 min. nc- TiO_2 films or FTO substrates were successively immersed in the Cd^{2+} and Te^{2-} solutions for 2 and 4 min, respectively, constituting one cycle of SILAR. The samples were rinsed with 1 mL of water between consecutive dipping to remove excess precursors. The SILAR cycle was repeated n times, the films are referred to as CdTe_n by the number of SILAR cycles. A nitrogen blanket was kept over the solutions during the deposition.

Photoelectrochemical Measurements. Photoelectrochemical measurements were collected in a three-electrode quartz cell using a CHI Model 630A electrochemical workstation with FTO/nc-TiO₂/Q-CdTe or FTO/Q-CdTe as the working electrode, a homemade Ag/AgCl (saturated KCl) as a reference electrode, and a 2 mm diameter Pt wire as an auxiliary electrode. Photoelectrochemical measurements were acquired in freshly prepared and deaerated Se²⁻ in 0.1 M NaOH electrolyte. The Se²⁻ hole scavenger was prepared in situ by reacting 0.1 M of Se powder with excess (0.2 M) NaBH₄ in 27 mL of distilled water and vigorously purging with N₂(g) until the red solution turned colorless. A 0.11 g amount of NaOH was then added to render the medium basic at pH ~ 12.8. A nitrogen blanket was kept above the electrolyte solution throughout the experiment to stabilize the Se²⁻ ions. In another set of experiments, aqueous sulfide electrolyte 0.1 M S²⁻/0.2 M NaOH was used. The electrolyte solution was purged with N₂(g) for at least 30 min, and a nitrogen blanket was kept above solution during measurements. For measurements under monochromatic light, the films were illuminated using a 300 W xenon lamp (model 66901 lamp housing, Oriel instruments) connected to a 1/4 m grating monochromator (Oriel Instruments, model 77200) to disperse the light. The lamp power spectrum and light intensity at the approximated position of the electrode were measured using a thermopile light detector and power meter (model 70260, Oriel Instruments) with average light measurements of 10 s.

Amperometric plots were acquired at -0.55 V (vs Ag/AgCl) with chopping of light, and the photocurrent was determined after subtraction of the dark current. The monochromatic incident-photon-to-current-conversion-efficiency (% IPCE) at a fixed voltage (*V*) was calculated according to (with *I* being the light intensity and *J* the current density):

$$\%IPCE(at\ V) = \frac{J_{@V}(A \cdot cm^{-2})}{I_{@λ}(W \cdot cm^{-2})} \times \frac{1240(eV \cdot nm)}{\lambda(nm)} \times 100$$

Film Characterization. SEM images and EDX spectra were acquired using TESCAN, VEGA 3 LMU with an OXFORD EDX detector (INCA XMAW20). The XRD spectra of the nc-TiO₂/CdTe₁₀ and FTO/CdTe₁₀ samples were collected using Bruker D8 Discover X-ray diffractometer operating at 40 kV/40 mA using Cu Kα radiation with a scanning speed of 0.5°/min and by referring to the PDF (powder diffraction file) database. Absorption spectra of the sensitized samples were collected before and after deposition using a UV-vis spectrophotometer (JASCO, V-570 UV/vis/NIR). An Ambios XP-1 profilometer was used to measure the thickness of the films. The obtained thickness for nc-TiO₂/CdTe₁₀ (*N* = 3) is 5.44 ± 0.20 μm and for FTO/CdTe₁₀ (*N* = 3) is 0.68 ± 0.14 μm.

■ ASSOCIATED CONTENT

■ Supporting Information

UV-vis spectra of CdTe₁₀ on FTO; chronoamperometry under chopped illumination at nc-TiO₂/CdTe₁₀ in S²⁻ and Se²⁻; UV-visible spectra, film photos, and EDX spectra of CdTe₁₀ on nc-TiO₂ before and after acquiring a photoaction spectrum in Se²⁻; photoaction and absorption spectra of CdTe₁₀CdSe₁ compared to CdTe₁₀ on nc-TiO₂ in Se²⁻; photoaction spectrum of CdTe₁₀ on nc-TiO₂ in alkaline NaBH₄ compared to Se²⁻ electrolyte; chronoamperometry plot at CdTe₁₀ on nc-TiO₂ in alkaline NaBH₄ upon 2 h continuous illumination at 500 nm and photo of the film and absorption spectrum after

experiment; photoaction spectra of CdTe₁₀ and CdTe₁₀CdSe₁ on FTO in Se²⁻. This material is available free of charge via the Internet at <http://pubs.acs.org>.

■ AUTHOR INFORMATION

Corresponding Author

*Tel: 9611350000. E-mail: Lara.Halaoui@aub.edu.lb.

Notes

The authors declare no competing financial interest.

■ ACKNOWLEDGMENTS

We thank the University Research Board at the American University of Beirut (grant 2011-13) and the Munib and Angela Masri Institute for Energy and Natural Resources (grant 2013-14) for financial support of this research. We also acknowledge the K. Shair Central Research Science Laboratory (CRSL) in the Faculty of Arts and Sciences at AUB for access to instruments.

■ REFERENCES

- (1) Mora-Seró, I.; Gimenez, S.; Fabregat-Santiago, F.; Gomez, R.; Shen, Q.; Toyoda, T.; Bisquert, J. Recombination in Quantum Dot Sensitized Solar Cells. *Acc. Chem. Res.* **2009**, *42*, 1848–1857.
- (2) Yu, W. W.; Qu, L.; Guo, W.; Peng, X. Experimental Determination of the Extinction Coefficient of CdTe, CdSe, and CdS Nanocrystals. *Chem. Mater.* **2003**, *15*, 2854–2860.
- (3) Wang, P.; Zakeeruddin, S. M.; Moser, J. E.; Humphry-Baker, R.; Comte, P.; Aranyos, V.; Hagfeldt, A.; Nazeeruddin, M. K.; Grätzel, M. Stable New Sensitizer with Improved Light Harvesting for Nanocrystalline Dye-Sensitized Solar Cells. *Adv. Mater.* **2004**, *16*, 1806–1811.
- (4) Vogel, R.; Pohl, K.; Weller, H. Sensitization of Highly Porous, Polycrystalline TiO₂ Electrodes by Quantum Sized CdS. *Chem. Phys. Lett.* **1990**, *174*, 241–246.
- (5) Vogel, R.; Hoyer, P.; Weller, H. Quantum-Sized PbS, CdS, Ag₂S, Sb₂S₃, and Bi₂S₃ Particles as Sensitizers for Various Nanoporous Wide-Bandgap Semiconductors. *J. Phys. Chem.* **1994**, *98*, 3183–3188.
- (6) Schaller, R. D.; Sykora, M.; Pietryga, J. M.; Klimov, V. I. Seven Excitons at a Cost of One: Redefining the Limits for Conversion Efficiency of Photons into Charge Carriers. *Nano Lett.* **2006**, *6*, 424–429.
- (7) Trinh, M. T.; Houtepen, A. J.; Schins, J. M.; Hanrath, T.; Pirus, J.; Knulst, W.; Goossens, A. P.; Siebbeles, L. D. In Spite of Recent Doubts Carrier Multiplication Does Occur in PbSe Nanocrystals. *Nano Lett.* **2008**, *8*, 1713–1718.
- (8) Beard, M. C.; Luther, J. M.; Semonin, O. E.; Nozik, A. J. Third Generation Photovoltaics based on Multiple Exciton Generation in Quantum Confined Semiconductors. *Acc. Chem. Res.* **2012**, *46*, 1252–1260.
- (9) Nozik, A. J. Nanoscience and Nanostructures for Photovoltaics and Solar Fuels. *Nano Lett.* **2010**, *10*, 2735–2741.
- (10) Stewart, J. T.; Padilha, L. A.; Qazilbash, M. M.; Pietryga, J. M.; Midgett, A. G.; Luther, J. M.; Beard, M. C.; Nozik, A. J.; Klimov, V. I. Comparison of Carrier Multiplication Yields in PbS and PbSe Nanocrystals: The Role of Competing Energy-Loss Processes. *Nano Lett.* **2011**, *12*, 622–628.
- (11) Hanna, M. C.; Beard, M. C.; Nozik, A. J. Effect of Solar Concentration on the Thermodynamic Power Conversion Efficiency of Quantum-Dot Solar Cells Exhibiting Multiple Exciton Generation. *J. Phys. Chem. Lett.* **2012**, *3*, 2857–2862.
- (12) Nozik, A. J. Quantum Dot Solar Cells. *Phys. E* **2002**, *14*, 115–120.
- (13) Nozik, A. Exciton Multiplication and Relaxation Dynamics in Quantum Dots: Applications to Ultrahigh-Efficiency Solar Photon Conversion. *Inorg. Chem.* **2005**, *44*, 6893–6899.

- (14) Hodes, G. Comparison of Dye- and Semiconductor-Sensitized Porous Nanocrystalline Liquid Junction Solar Cells. *J. Phys. Chem. C* **2008**, *112*, 17778–17787.
- (15) Luther, J. M.; Law, M.; Beard, M. C.; Song, Q.; Reese, M. O.; Ellingson, R. J.; Nozik, A. J. Schottky Solar Cells Based on Colloidal Nanocrystal Films. *Nano Lett.* **2008**, *8*, 3488–3492.
- (16) Istrate, E.; Hoogland, S.; Sukhovatkin, V.; Levina, L.; Myrskog, S.; Smith, P. W.; Sargent, E. H. Carrier Relaxation Dynamics in Lead Sulfide Colloidal Quantum Dots. *J. Phys. Chem. B* **2008**, *112*, 2757–2760.
- (17) Kongkanand, A.; Tvrdy, K.; Takechi, K.; Kuno, M.; Kamat, P. V. Quantum Dot Solar Cells. Tuning Photoresponse Through Size and Shape Control of CdSe-TiO₂ Architecture. *J. Am. Chem. Soc.* **2008**, *130*, 4007–4015.
- (18) Leschkies, K. S.; Divakar, R.; Basu, J.; Enache-Pommer, E.; Boercker, J. E.; Carter, C. B.; Kortshagen, U. R.; Norris, D. J.; Aydil, E. S. Photosensitization of ZnO Nanowires with CdSe Quantum Dots for Photovoltaic Devices. *Nano Lett.* **2007**, *7*, 1793–1798.
- (19) Lee, H. J.; Yum, J.-H.; Leventis, H. C.; Zakeeruddin, S. M.; Haque, S. A.; Chen, P.; Seok, S. I.; Grätzel, M.; Nazeeruddin, M. K. CdSe Quantum Dot-Sensitized Solar Cells Exceeding Efficiency 1% at Full-Sun Intensity. *J. Phys. Chem. C* **2008**, *112*, 11600–11608.
- (20) Shen, Q.; Kobayashi, J.; Diguna, L. J.; Toyoda, T., Effect of ZnS Coating on the Photovoltaic Properties of CdSe Quantum Dot-Sensitized Solar Cells. *J. Appl. Phys.* **2008**, *103*.
- (21) Bang, J. H.; Kamat, P. V. Quantum Dot Sensitized Solar Cells. A Tale of Two Semiconductor Nanocrystals: CdSe and CdTe. *ACS Nano* **2009**, *3*, 1467–1476.
- (22) Yue, G.; Wu, J.; Xiao, Y.; Lin, J.; Huang, M.; Lan, Z.; Fan, L. CdTe Quantum Dots-Sensitized Solar Cells Featuring PCBM/P3HT as Hole Transport Material and Assistant Sensitizer Provide 3.40% Efficiency. *Electrochim. Acta* **2012**, *85*, 182–186.
- (23) Ellis, A. B.; Kaiser, S. W.; Bolts, J. M.; Wrighton, M. S. Study of n-Type Semiconducting Cadmium Chalcogenide-Based Photoelectrochemical Cells Employing Polychalcogenide Electrolytes. *J. Am. Chem. Soc.* **1977**, *99*, 2839–2848.
- (24) Salant, A.; Shalom, M.; Hod, I.; Faust, A.; Zaban, A.; Banin, U. Quantum Dot Sensitized Solar Cells with Improved Efficiency Prepared Using Electrophoretic Deposition. *ACS Nano* **2010**, *4*, 5962–5968.
- (25) Kamat, P. V. Quantum Dot Solar Cells. Semiconductor Nanocrystals as Light Harvesters. *J. Phys. Chem. C* **2008**, *112*, 18737–18753.
- (26) McGregor, S.; Dharmadasa, I.; Wadsworth, I.; Care, C. Growth of CdS and CdTe by Electrochemical Technique for Utilisation in Thin Film Solar Cells. *Opt. Mater.* **1996**, *6*, 75–81.
- (27) Smith, N. J.; Emmett, K. J.; Rosenthal, S. J. Photovoltaic Cells Fabricated by Electrophoretic Deposition of CdSe Nanocrystals. *Appl. Phys. Lett.* **2008**, *93*, 043504.
- (28) Lee, W.; Min, S. K.; Dhas, V.; Ogale, S. B.; Han, S.-H. Chemical Bath Deposition of CdS Quantum Dots on Vertically Aligned ZnO Nanorods for Quantum Dots-Sensitized Solar Cells. *Electrochem. Commun.* **2009**, *11*, 103–106.
- (29) Prabakar, K.; Seo, H.; Son, M.; Kim, H. CdS Quantum Dots Sensitized TiO₂ Photoelectrodes. *Mater. Chem. Phys.* **2009**, *117*, 26–28.
- (30) Badawi, A.; Al-Hosiny, N.; Abdallah, S.; Negm, S.; Talaat, H. Tuning Photocurrent Response Through Size Control of CdTe Quantum Dots Sensitized Solar Cells. *Sol. Energy* **2013**, *88*, 137–143.
- (31) Lee, H.; Wang, M.; Chen, P.; Gamelin, D. R.; Zakeeruddin, S. M.; Grätzel, M.; Nazeeruddin, M. K. Efficient CdSe Quantum Dot-Sensitized Solar Cells Prepared by an Improved Successive Ionic Layer Adsorption and Reaction Process. *Nano Lett.* **2009**, *9*, 4221–4227.
- (32) Guijarro, N. S.; Lana-Villarreal, T.; Shen, Q.; Toyoda, T.; Gómez, R. Sensitization of Titanium Dioxide Photoanodes with Cadmium Selenide Quantum Dots Prepared by SILAR: Photoelectrochemical and Carrier Dynamics Studies. *J. Phys. Chem. C* **2010**, *114*, 21928–21937.
- (33) Cheng, S.; Fu, W.; Yang, H.; Zhang, L.; Ma, J.; Zhao, H.; Sun, M.; Yang, L. Photoelectrochemical Performance of Multiple Semiconductors (CdS/CdSe/ZnS) Cosensitized TiO₂ Photoelectrodes. *J. Phys. Chem. C* **2012**, *116*, 2615–2621.
- (34) Bayram, S.; Halaoui, L. Amplification of Solar Energy Conversion in Quantum-Confined CdSe-Sensitized TiO₂ Photonic Crystals by Trapping Light. *Part. Part. Syst. Charact.* **2013**, *30*, 706–714.
- (35) Klayman, D. L.; Griffin, T. S. Reaction of Selenium with Sodium Borohydride in Protic Solvents. A Facile Method for the Introduction of Selenium into Organic Molecules. *J. Am. Chem. Soc.* **1973**, *95*, 197–199.
- (36) Lee, H. J.; Bang, J.; Park, J.; Kim, S.; Park, S.-M. Multilayered Semiconductor (CdS/CdSe/ZnS)-Sensitized TiO₂ Mesoporous Solar Cells: All Prepared by Successive Ionic Layer Adsorption and Reaction Processes. *Chem. Mater.* **2010**, *22*, 5636–5643.
- (37) Guijarro, N.; Lutz, T.; Lana-Villarreal, T.; O'Mahony, F.; Gómez, R.; Haque, S. A. Toward Antimony Selenide Sensitized Solar Cells: Efficient Charge Photogeneration at Spiro-OMeTAD/Sb₂Se₃/Metal Oxide Heterojunctions. *J. Phys. Chem. Lett.* **2012**, *3*, 1351–1356.
- (38) Mora-Seró, I.; Bisquert, J.; Dittrich, T.; Belaidi, A.; Susha, A. S.; Rogach, A. L. Photosensitization of TiO₂ Layers with CdSe Quantum Dots: Correlation between Light Absorption and Photoinjection. *J. Phys. Chem. C* **2007**, *111*, 14889–14892.
- (39) Trindade, T.; O'Brien, P.; Pickett, N. L. Nanocrystalline Semiconductors: Synthesis, Properties, and Perspectives. *Chem. Mater.* **2001**, *13*, 3843–3858.
- (40) Chakrapani, V.; Baker, D.; Kamat, P. V. Understanding the Role of the Sulfide Redox Couple (S²⁻/S_n²⁻) in Quantum Dot-Sensitized Solar Cells. *J. Am. Chem. Soc.* **2011**, *133*, 9607–9615.